Virtual Reality
https://doi.org/10.1007/s10055-023-00863-3

ORIGINAL ARTICLE

A systematic evaluation of an RTK-GPS device for wearable augmented reality

Francesco De Pace[1] · **Hannes Kaufmann**[1]

Received: 14 July 2022 / Accepted: 11 September 2023

Abstract
Global Positioning Satellite (GPS) systems sample points on the Earth's surface with meter accuracy. Real-Time Kinematic (RTK) devices improve GPS performances by providing real-time correction data from ground stations, achieving centimeter accuracy. Reliable tracking approaches are essential for Augmented Reality (AR) applications, especially for outdoor scenarios, which still present unsolved challenges. AR handheld tracking capabilities have been greatly improved by integrating visual tracking approaches with RTK devices, whereas little is known about combining wearable AR interfaces with RTK systems. Although wearable AR devices are intrinsically designed for AR applications, their performance dramatically reduces in large outdoor areas, comprising the user experience. Hence, this paper provides a rigorous evaluation of a small-size RTK device that does not need any additional software integration to collect positional data. The main goal of the assessment is to verify whether its integration with a wearable AR device is advantageous or not. The evaluation has been performed considering both static and dynamic scenarios in open-sky and urban areas. The results show that the RTK device can achieve 1 cm accuracy when used in open-sky areas. In contrast, its accuracy dramatically reduces in the proximity of buildings and obstacles, showing average errors ranging from 76 to 2561%. Since wearable AR devices have an average accuracy of 2 cm, the outcomes indicate that RTK devices should be combined with wearable AR devices only when the RTK device is far from obstacles. On the contrary, the positional data should be completely avoided when barriers surround the RTK device.

Keywords Augmented reality · Outdoor tracking · Real-time kinematic · GPS

1 Introduction

Augmented Reality (AR) dates back to the sixties when Sutherland proposed a Head Mounted Device (HMD) capable of overlaying virtual contents on real-world objects (Sutherland 1968). Since then, AR has been increasingly researched and improved by academic entities and industries, becoming one of the key-technologies used in several fields and domains (Mekni and Lemieux 2014).

Nowadays, AR applications are being developed using three main interfaces: (i) projected, (ii) handheld, and (iii) wearable. Due to their intrinsic differences, each interface has its own best application area. As an example, AR projected interfaces are usually used for indoor static and semi-static tasks, that is, the user's movements are limited to the projection area. On the contrary, handheld and wearable interfaces can be easily employed for applications that allow the users to physically move, both in indoor and outdoor areas. Regarding outdoor locations, AR interfaces have been deeply researched for several application domains, such as training (Lucero-Urresta et al. 2021), cultural heritage (Gleue and Dähne 2001) and learning (Pombo et al. 2019). Independently of the application, AR interfaces are affected by several well-known limitations. Occlusions prevent users from clearly distinguishing virtual and real contents, virtual assets might be hard to be spotted due to a very narrow field-of-view (especially for wearable devices) and limited tracking capabilities may negatively affect visualization of the virtual contents (for a detailed discussion related

✉ Francesco De Pace
francesco.pace@tuwien.ac.at

Hannes Kaufmann
hannes.kaufmann@tuwien.ac.at

[1] Institute of Visual Computing and Human-Centered Technology, TU Wien, Favoritenstrasse 9-11, Vienna 1040, Austria

Published online: 16 October 2023

to AR limitation please refer to Van Krevelen and Poelman (2010), Nazri and Rambli (2014)).

Especially for AR outdoor applications, tracking is one of the current research hot topics and it is widely researched by both academics and industries (Reitmayr and Drummond 2006; Blanco-Pons et al. 2019). Continuous localization of the users is usually carried out by using Global Positioning System (GPS) (Kamat and Behzadan 2006; Kurkovsky et al. 2012; Han et al. 2013). GPS is a satellite-based system developed by the USA. It is composed of 24 satellites that orbit at medium altitudes around the Earth (Hegarty 2017). Although it provides 3D positions, time, and velocity data, several drawbacks limit the GPS systems to meter accuracy (Morales and Tsubouchi 2007). Differential GPS (DGPS) systems overcome these limitations by using correction signals generated from additional base stations, achieving less than 1 m accuracy whether real-time, centimeter accuracy can be reached by employing Real-Time Kinematic (RTK) GPS devices (Gan-Mor et al. 2007). Although the primary activities of handheld devices (e.g., smartphones or tablets) are not AR-related (e.g., sending messages, making calls, etc.), they are heavily used for outdoor AR scenarios, though they suffer from poor tracking capabilities and thus, they are improved by combining GPS data with Simultaneous Localization and Mapping (SLAM) techniques (Agrawal and Konolige 2006; Speroni et al. 2018). However, AR handheld interfaces are not meant for applications that require low image generation delay, a high sense of immersion, and hand-free capabilities. Instead, wearable AR devices are designed for such scenarios; they are equipped with dedicated sensors (e.g. RGB, or RGB-D sensors) that natively improve the AR experience without using additional fusion algorithms. Specifically, wearable AR devices (e.g., the Microsoft HoloLens 2[1] or the Magic Leap 2[2]) utilize Visual Simultaneous Localization and Mapping (vSLAM) techniques to generate a map of the surrounding and determine their own location within it Ungureanu et al. (2020), Zari et al. (2023). However, these algorithms face limitations when encountering repetitive patterns and are primarily designed for indoor use (Taketomi et al. 2017). Hence, the positional data obtained from highly accurate RTK-GPS systems (henceforth, the term *RTK-GPS* will be used to address RTK GPS systems whereas the term *GPS* will be employed to indicate traditional GPS devices) could potentially overcome these limitations, opening up the potential to use wearable AR devices in environments lacking textures or characterized by ambiguous features, such as deserts or extraterrestrial landscapes (Zheng et al. 2022). From an application perspective, the integration of RTK-GPS devices will improve AR applications in at least two different ways. Firstly, end-users will have the capability to accurately position virtual objects in textureless and ambiguous environments, without facing tracking issues. Secondly, it will foster the development of multi-user AR applications by enabling the accurate tracking of multiple users, each equipped with an RTK-GPS combined with a wearable AR device. However, there is still little research that has addressed this topic. While GPS-AR handheld systems have been deeply investigated and researched, there is a lack of research that has verified whether it is advantageous or not to integrate highly accurate GPS systems with wearable AR devices. This research considers only small-size, highly accurate, commercially available RTK-GPS devices that provide *as is* accurate positional data without the necessity of integrating additional hardware or software. Hence, this paper evaluates the accuracy of a small-portable RTK-GPS device, considering both static and dynamic scenarios (i.e., the RTK-GPS device remains fixed at a specific location in static conditions while it keeps changing its physical location in dynamic conditions). The results will be useful for understanding whether wearable AR devices should integrate or not RTK-GPS devices when used in outdoor, ambiguous areas.

2 State of the art

Several works have assessed the accuracy of small-size RTK-GPS devices for static conditions. Wiśniewski et al. (2013) evaluated the open-source RTKLIB library for real-time and post-processed positioning data collection. They showed that obtaining centimeter accuracy with low-cost modules is possible after an initial calibration phase of approximately 8 min. Teunissen et al. (2014) show that a combination of an RTK-GPS and the BeiDou Navigation Satellite System (BDS) improves the cut-off elevation angle range. Similar outcomes can be found in Odolinski et al. (2015). The research carried out in Odolinski and Teunissen (2017) demonstrates that low-cost receivers can achieve accuracy levels comparable to those of costly survey-grade devices in static conditions. The surrounding inferences are analyzed in Chiuman et al. (2019) considering a jungle environment. The outcomes illustrate that it is possible to obtain centimeter and sub-meter accuracy depending on the signal strength, even in jungle areas.

In addition to small-size RTK-GPS devices, large-size systems have also been researched and assessed. Bakuła et al. (2014) compared an RTK-GPS system with a rapid static one showing that the latter is much more reliable and accurate than the RTK-GPS system when used in forest environments. The authors of Safrel et al. (2018) demonstrate that in dense areas, a total station can achieve higher levels

[1] https://www.microsoft.com/en-us/hololens.

[2] https://www.magicleap.com/magic-leap-2.

of accuracy with respect to an RTK-GPS system [(Mahdi et al. 2018) presents a similar comparison].

RTK-GPS performances have also been verified considering dynamic conditions, that is, the RTK-GPS devices collect positional data while changing their physical location. Kluga et al. (2014) suggest that it is possible to obtain centimeter accuracy using moving RTK-GPS systems. However, their results lack statistical data analysis to identify possible outliers, and they evaluated only devices with low-frequency updates (0.1Hz and 1Hz). In Henkel et al. (2016), the authors propose an interesting RTK-GPS/GLONASS positioning system for low-cost receivers. They show that their approach, combined with a multi-GNSS receiver, an inertial sensor, a patch antenna, and a barometer, can achieve millimeter-to-centimeter-level accuracy. The authors of Ng et al. (2018) assessed a large-size RTK-GPS system in dynamic conditions, considering both flat and uneven landscapes. The primary outcomes indicate that when moving through a hillside landscape (with slopes that do not exceed 30°), the RTK-GPS system performs as well as in the flat landscape scenario. A low-cost GPS-RTK receiver and a state-of-the-art module are compared in Zhang et al. (2019), integrating the US GPS system with the Chinese BeiDou one. In dynamic conditions, the GPS-RTK module achieves an accuracy of 20 cm, with an update frequency bounded to 5Hz. Finally, Tomaszewski et al. (2020) analyzed how distance from the reference station affects RTK-GPS accuracy. The results indicate that it is possible to obtain centimeter accuracy within 82 Km from the reference station.

Several research projects have successfully integrated RTK-GPS devices with handheld AR interfaces (Schall et al. 2009; Stranner et al. 2019; Guarese and Maciel 2019; Niu et al. 2020; Singh et al. 2020). Schall et al. (2009) used the Kalman filter to fuse data from various sensors (IMU and camera) with RTK-GPS positional data, achieving submeter positional accuracy. The authors of Stranner et al. (2019) compared a low-cost DGPS device (combined with IMU, altimeter, and camera) with a highly accurate GPS receiver in static conditions. Their results show a maximum accuracy error of 5 cm with a maximum resolution of 2 cm. In Guarese and Maciel (2019), a wearable AR device has been compared with an AR handheld system combined with a traditional GPS module. The main outcomes show that the handheld system required less cognitive and physical workloads and better usability than the wearable one. Niu et al. (2020) proposed a Visual SLAM solution combined with an RTK-GPS system for a handheld AR device. The results indicate that the RTK-GPS device can achieve 1 m accuracy in open-sky areas, whereas the accuracy decreases to 5 m in areas covered by several obstacles. Singh et al. (2020) developed a collaborative virtual environment. The AR user interacts using a handheld device tracked with a visual SLAM approach combined with a traditional GPS. The authors compare their tracking solution with a conventional GPS obtaining a more stable and smooth trajectory than the one generated by the standard GPS.

The first preliminary experiments that combined GPS systems with wearable AR interfaces date back to the nineties when Feiner et al. (1997) improved a wearable outdoor tracking system using a DSM GPS device. The same system was used for the MARS project (Höllerer et al. 1999). Later, Thomas et al. (2000) proposed the well-known ARQuake game, one of the AR games that employed GPS data to track the users' positions in outdoor areas. Over the years, GPS AR wearable systems have been increasingly researched and improved, and it is possible to find several research projects. As an example, the authors of Piekarski et al. (2003) combined a DGPS wearable AR system with the famous indoor tracking framework ARToolkit for an indoor-outdoor navigation system. GPS systems have also been successfully employed for monitoring and assisting military personnel (Tache et al. 2012; Menozzi et al. 2014). Recently, the impact of the integration of a GPS device with the Microsoft HoloLens device on neuroplastic changes and navigation abilities has been investigated in Fajnerová et al. (2018) whereas the authors of Isrie et al. (2018) propose an AR interface that displays the user's path by means of a wearable AR device.

From the state-of-the-art analysis, it is clear that most of the experiments have primarily focused on assessing the performance of RTK-GPS combined with AR handheld interfaces, particularly under static conditions (Stranner et al. 2019). Moreover, the achieved accuracies in these experiments are not sufficient for meeting the requirements of wearable AR devices, with results falling within the range of meter or submeter accuracy (Schall et al. 2009; Niu et al. 2020). Additionally, some studies have not conducted comprehensive evaluations of the system capabilities Guarese and Maciel (2019). These limitations in the existing research highlight the need for further investigation and exploration in the field of RTK-GPS integration with wearable AR devices. The inaccuracies introduced by traditional GPS systems can significantly impact the tracking accuracy of wearable AR systems. Consequently, RTK-GPS systems have the potential to enhance the tracking capabilities of wearable AR devices when used in outdoor environments. Specifically, the highly accurate positional data of the RTK-GPS devices could overcome the limitations of the vSLAM algorithms when used in ambiguous, textureless, and repetitive environments (e.g., deserts or extraterrestrial landscapes). Furthermore, it will be possible to accurately track multiple users, thus fostering the development of multi-user AR applications. However, it is necessary to understand which are the strengths and limitations of the RTK-GPS systems. The RTK-GPS system proposed in Henkel et al. (2016) shows remarkable capabilities but requires several additional devices to operate (thus,

it is not a self-contained, portable solution). Zhang et al. (2019) discuss an interesting experiment, but their system is bounded to a maximum frequency update of 5Hz. The only work that integrates an RTK-GPS with a wearable AR system can be found in Ling et al. (2019), but it has not been assessed and tested. Hence, the work presented in this paper analyzes a small-size, self-contained, commercially available RTK-GPS device that does not need any additional integration to produce highly precise positional data with a frequency update of 10Hz. The assessment involves both static and dynamic conditions considering two different environments to verify the device's strengths and limits when used in open-sky and high-dense areas. Through this analysis, we aim to gain insights into the strengths and limitations of integrating RTK-GPS devices with wearable AR systems and understand the conditions under which such integration would be beneficial.

3 The system

This section introduces the hardware and software components used for the RTK-GPS assessment.

3.1 Hardware

The evaluated RTK-GPS is the Smartphone RTK device from the REDCatch company.[3] It is a small-size, self-contained RTK GNSS receiver that operates using both L1 and L2 frequencies. By connecting it to an Android smartphone, it starts receiving GPS and correctional data that are automatically combined, obtaining highly precise positional data without requiring additional software implementation. The RTK-GPS device can be connected to the smartphone through USB or Bluetooth; the USB option was preferred for performance and reliability reasons (Fig. 1 shows the RTK-GPS device connected through USB to an Android smartphone).

The Android smartphone is the Samsung S8 with Android 9 (Pie).

3.2 Software

The proposed system includes two different Android applications: (i) the Ntrip REDCatch App and (ii) a custom application. The former is developed by the REDCatch company, and its primary role is to receive highly precise positional data. It is possible to change the frequency update (set to 10Hz) and the user can set the IP and port addresses of the chosen service provider required to receive the correction

Fig. 1 The REDCatch Smartphone RTK device (on the left) connected through USB to an Android Samsung S8 smartphone (on the right)

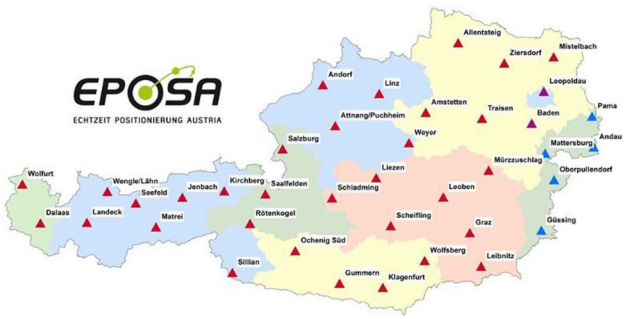

Fig. 2 The EPOSA network infrastructure. Taken from https://www.eposa.at/infrastruktur, accessed on the 1st of October 2023

data. EPOSA (Echtzeit Positionierung Austria)[4] is the service provider; it offers high-quality satellite-based positional services using all global satellite systems (Beidou, GALILEO, GLONASS, and GPS). The EPOSA network comprises more than 40 reference stations covering the entire Austrian territory (Fig. 2). The correction data are sent over the Internet to the REDCatch App that combines them with the GPS data received by the RTK-GPS device.

To complete the REDCatch App configuration, the user must select a mounting point. The RTK-3 (pure RTK correction data) mounting point has been chosen for this evaluation. Finally, the REDCatch App can replace the smartphone's internal GNSS data with its accurate positional ones by enabling the Mock-location feature of the Android

[3] https://www.redcatch.at/smartphonertk/.

[4] https://www.eposa.at/englisch.

developer mode, allowing any custom Android application to easily read the accurate positional data.

In order to assess the RTK-GPS accuracy, a custom Android application has been developed using Android Studio[5] as Integrated Development Environment. The Android application can act in two different modalities, depending on the number of smartphones (and related GPS-RTK devices): (i) data saving modality (DSM) and (ii) real-time modality (RTM). In DSM, one smartphone collects the positional data mocked by the REDCatch app, saving them on a text file. The RTM modality requires two distinct smartphone-RTK-GPS devices. One smartphone acts as a TCP client: it reads the mocked positional data on a dedicated thread, storing them on a synchronized list. Another thread reads from the list the collected data, sending them to a TCP server. The other smartphone acts as a TCP server and receives the client data, also collecting its own mocked positional data. The two modalities were used in the test session, depending on the type of evaluation (more details in Sect. 5.1).

4 Preliminary test

Prior to the accuracy evaluation, two users were instructed to walk in two different locations while collecting positional data using the DSM modality. Each user was equipped with an RTK-GPS device, which was connected to their mobile phone via USB. The primary objective was to analyze the users' walking paths by visually examining the data plotted on Google Maps. The selected locations presented noticeable environmental differences: the location shown in Fig. 3a (LOC_A) is located in the courtyard of the University campus. It consists of a highly dense area, surrounded by many trees and buildings. On the contrary, the location shown in Fig. 3b (LOC_B) is a wide open-sky area, close to a lake, which is not surrounded by any kind of environmental obstacles. The users were asked to walk along two identical 30 m predefined paths in both LOC_A and LOC_B, repeating the process four times.

By visually inspecting the positional data (Fig. 4), it can be seen immediately that LOC_B paths provided a better approximation of the actual track compared to LOC_A. Furthermore, the data from LOC_B exhibited repetitive trajectories, while the paths in LOC_A were irregular, displaying significant variations among the trajectories. Although the initial tests indicate potential inaccuracies in the LOC_A data, a precise evaluation of the RTK-GPS devices' accuracy cannot be determined without ground-truth data. Hence, the next Section presents a rigorous analysis aimed at assessing the actual accuracy of the RTK-GPS devices. This analysis

(a) LOC_A: the University courtyard.

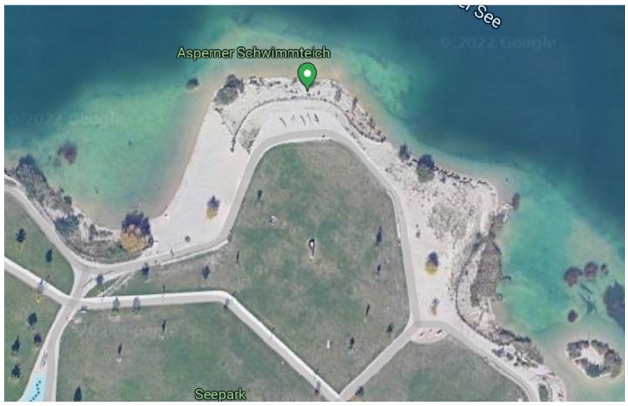

(b) LOC_B: the open-sky area.

Fig. 3 The RTK-GPS device has been tested in two distinct environments: a high-dense urban area (**a**) and an open-sky location (**b**)

seeks to truthfully determine the conditions under which these devices can be utilized for developing AR applications.

5 Metrics and possible limitations

In this section, the metrics used to evaluate the RTK-GPS accuracy are presented and discussed as well as the current limitations of the chosen metrics.

5.1 Metrics

Five different parameters were collected and analyzed: (i) the dispersion from the average value (DAV), (ii) the accuracy in terms of the relative distance between two different RTK-GPS devices (ACC), (iii) the GPS quality from the GNGGA message of the NMEA protocol (GPS_Q), (iv) the number of satellites in use from the GNGGA message (SAT_U), and (v) the number of satellites in view from the GPGSV message (SAT_V). When not discussed separately, the last three parameters will be referred to as SAT_D.

[5] https://tinyurl.com/4ac9bh3x.

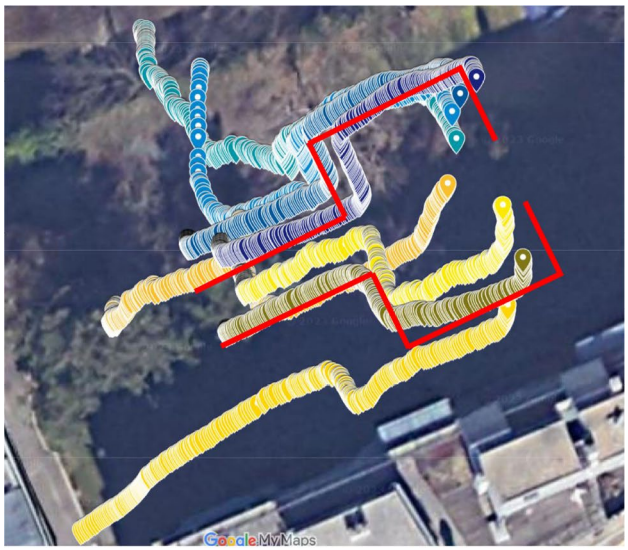

(a) The LOC_A paths.

(b) The LOC_B paths.

Fig. 4 The red lines represent the actual paths, whereas the trajectories of the two users are visualized using blue and yellow color schemes, respectively

The tests consider both static and dynamic conditions. All five parameters were analyzed during the static condition whereas DAV was omitted from the dynamic session.

For analyzing DAV in the static condition, one RTK-GPS device (along with the Android smartphone) was placed in a fixed position for a pre-defined amount of time. The smartphone acted in DSM modality, collecting the positional data. ACC was assessed using two different RTK-GPS devices (with two Samsung S8) in both static and dynamic conditions. They were placed in two different positions at a known distance $L = 55$ cm that was compared with their relative distance computed using the collected positional data, thus assessing the system accuracy. The comparison of tracking data with a pre-defined value (i.e., the L distance) is a well-known procedure that proves effective in assessing the accuracy of tracking systems (Pintaric and Kaufmann 2007; Jakus et al. 2014; Kluga et al. 2014). The specific value ($L = 55$ cm) was chosen for practical reasons; in fact, to assess the accuracy under dynamic conditions, a rotating platform was constructed, and a rigid metal bar of length L was attached to it. To ensure a rigid system with no deformation of the bar, a length of approximately half a meter ($L = 55$ cm) was selected. This choice also facilitated the attachment of the bar to the motors of the rotating platform. ACC was computed using both DSM and RTM. In DSM, the two smartphones independently collected the positional data, used later for calculating the relative distance during a post-processing data analysis phase. In RTM, when the server receives the client data, it computes on the fly the relative distance, storing them on a text file. For evaluating ACC in static and dynamic conditions, the RTK-GPS devices have been attached to a rigid metal bar fixed to a circular rotating platform. The devices were positioned at the known distance L. During the static condition, the rotating platform was kept fixed, whereas, during the dynamic condition, it started rotating at a very slow velocity. Independently of the modality, condition, and assessed parameter, SAT_D were always collected by logging the NMEA messages received by the REDCatch application (for ACC, the NMEA messages of both smartphones were stored). Table 1 summarizes the parameter-condition-modality relations.

Table 1 Given a condition and a parameter, each cell highlights the modality used to collect and analyze the data

	Static	Dynamic
DAV	DSM	
ACC	DSM	DSM
	RTM	RTM
SAT_D	Log	Log

5.1.1 GPS distance computation

A single GPS coordinate P can be expressed in terms of latitude ϕ and longitude λ coordinates, $P(\phi, \lambda)$. Given two distinct GPS coordinates P_1 and P_2 expressed in radians, their relative distance can be computed using at least three different methods: (i) Haversine formula, (ii) spherical law of cosines and (iii) equirectangular approximation. All three methods have been used to assess ACC and they have been implemented as follows.

Haversine distance D_H:

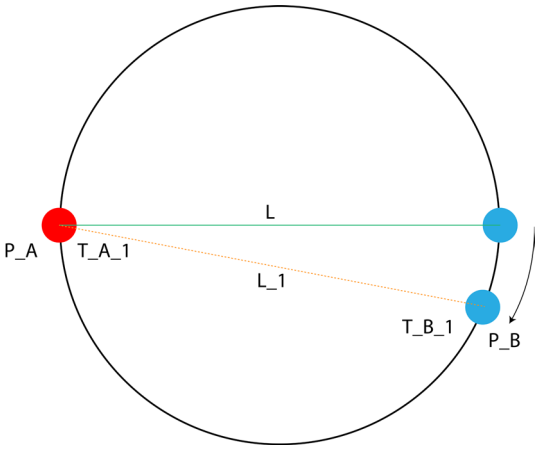

Fig. 5 The red and blue circles are the positions of the A and B devices. The green line represents the true distance whereas the yellow line represents the distance computed without synchronization

$$\begin{aligned} a &= sin^2(\delta\phi/2) + cos\phi_1 cos\phi_2 sin^2(\delta\lambda/2) \\ c &= 2atan2\left(\sqrt{a}, \sqrt{1-a}\right) \\ D_H &= Rc \end{aligned} \tag{1}$$

where $\delta\phi$ is the latitude difference, $\delta\lambda$ is the longitude difference and R is the Earth radius ($R = 6371$ Km).

Equirectangular approximation distance D_E:

$$\begin{aligned} a &= \delta\lambda cos((\phi_1 + \phi_2)/2) \\ D_E &= R\sqrt{a^2 + \delta\phi^2} \end{aligned} \tag{2}$$

Spherical law of cosine distance D_S:

$$D_S = acos(sin\phi_1 sin\phi_2 + cos\phi_1 cos\phi_2 cos\delta\lambda)R \tag{3}$$

5.2 Limitation of the accuracy metric

The proposed work presents a limitation in that distances between two different RTK-GPS devices have been computed using Eqs. 1, 2, and 3 in both static and dynamic conditions without relying on a synchronization system.

Referring to Fig. 5, two not-synchronized RTK-GPS devices (A and B) are fixed on the rigid metal bar at distance L. While the platform is rotating, P_A (the GPS position of the A device) is received at time T_{A_1} and it is used to compute the distance with P_B received at time T_{B_1}, with $T_{A_1} ! = T_{B_1}$. Therefore, it will compute the L_1 distance, biasing the results. To mitigate the effects of this drawback, two different strategies have been adopted. Firstly, the platform rotates very slowly, minimizing the possible positional errors (the positional data are also received with high frequency which further mitigates the lack of synchronization). Secondly, when distances are not computed with RTM mode, the data have been manually synchronized during the post-processing data analysis step, using the location Unix epoch time value.[6] The positional data time values are set from the clock in use by the considered satellite constellation. Since A and B were positioned very close to each other ($L = 55$ cm), it is very likely that the two devices received the data from the same satellite constellation, thus referring to the same clock.

In order to present a truthful analysis, both not-synchronized and synchronized results will be presented and discussed, highlighting differences in the results.

Table 2 Given a location and time period, PT was performed only in static condition using DSM, AT was performed in both conditions using DSM and RTM

	Static	Dynamic
PT	DAV (DSM)	
AT	ACC (DSM, RTM)	ACC (DSM, RTM)

6 Test

In order to assess the performances of the REDCatch RTK-GPS device, several tests have been carried out in LOC_A and LOC_B locations.

The tests were divided into (i) Positional (PT) and (ii) Accuracy (AT) tests. The former analyzed DAV with related SAT_D, the latter assessed ACC with related SAT_D.

Given one location, PT has been carried out only in static conditions, using DSM modality (1 test in total). On the other hand, AT was performed in both static and dynamic conditions, using both DSM and RTM modalities (4 tests in total). Each test was performed for two different amounts of time (1 and 5 min). Table 2 summarizes the number of tests performed considering a specific location and amount of time.

PTs were structured as follows. An operator placed the RTK-GPS device (and related smartphone) in a fixed position. Then, they launched the REDCatch (with log enabled) app and the custom Android application (DMS modality), saving the positional data for a specific amount of time. For ATs, the two RTK-GPS (and smartphones) were fixed to the rigid metal bar attached to the rotating platform. In the static condition, DMS modality, the operator launched the REDCatch and the custom Android applications on both smartphones, starting to collect the GPS data. In the static condition, RTM modality, the two smartphones were connected to the same Local Area Network, and one of the smartphones (the client) is connected to the other one (the server). Then,

[6] https://tinyurl.com/5xy7t7mk.

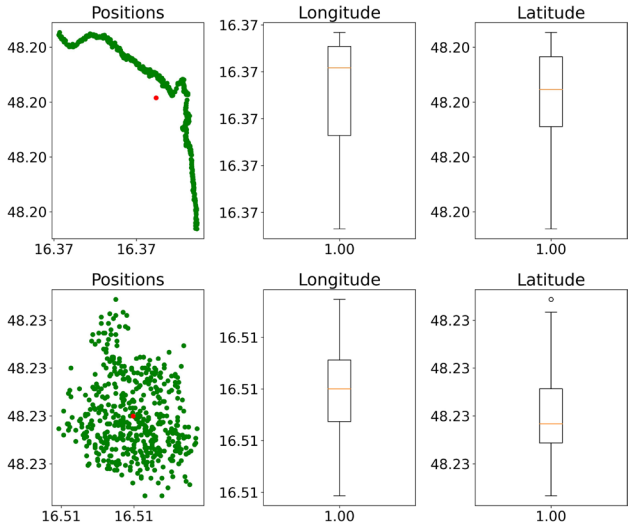

(a) PT T_1 data.

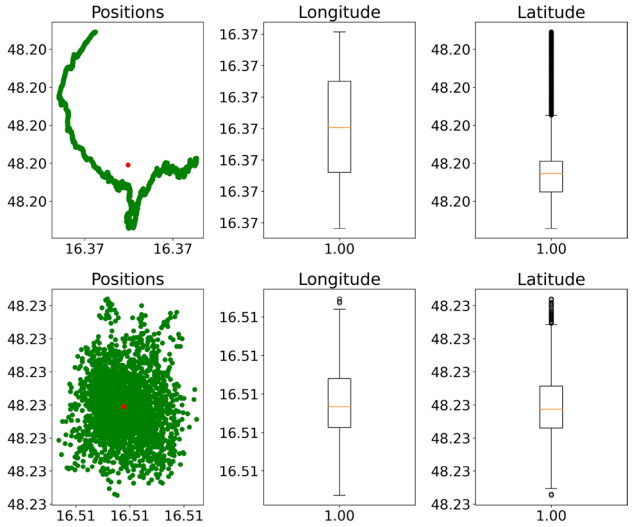

(b) PT T_5 data.

Fig. 6 The PT data. Referring to both figures, the first rows show LOC_A data, the second rows LOC_B data. The red dots (*Positions* plots) represent the mean values

the operator launched the REDCatch application (on both devices), allowing the server to compute and save the data in real-time. In the dynamic condition, the tests were structured as in static condition with the difference of the rotating platform. The operator started the rotating platform after launching the REDCatch and custom Android applications.

6.1 PT results

PT data have been collected independently in both locations (LOC_A and LOC_B) for two different periods ($T_1 = 1$ min and $T_5 = 5$ min). With an update frequency of 10Hz, the RTK-GPS device collected 594 values for LOC_A T_1, 593 for LOC_B T_1, 2985 for LOC_A T_5 and 2989 for LOC_B T_5. The data have been then filtered out to remove any missing values. Only LOC_B T_5 presented one missing value, thus obtaining a total amount of data equal to 2988. Figure 6a and b shows the final PT data collected for T_1 and T_5, respectively.

The first rows of both figures present LOC_A PT data while LOC_B PT data are plotted on the second rows. Considering one row, the first plot shows the positional data while the remaining two illustrate the latitude and longitude Interquartile Ranges (IQRs), respectively. By qualitatively analyzing the data, it is clear that LOC_B PT data are much more concentrated around the mean value than the LOC_A ones. The latitude and longitude values of LOC_A PT T_1 tend to be more upper skewed than the LOC_B PT T_1 data, which on the contrary, are uniformly distributed around the mean value. Similarly, Fig. 6b shows that the latitude and longitude LOC_A PT values are more spread out than the LOC_B ones, especially the latitude data that present several outliers.

In order to perform a truthful analysis, the outliers have been filtered out using the IQRs. Specifically, the latitude and longitude LOC_A and LOC_B PT values (T_1 and T_5) have been filtered using the following condition:

$$Q1_C - 1.5 * IQR_C \leq C_i \leq Q3_C + 1.5 * IQR_C \quad 1 \leq i \leq N \tag{4}$$

where C represents a component (latitude or longitude), $Q1_C$ is the component's first IQR, $Q3_C$ is the component's third IQR, IQR_C is the IQR ($IQR_C = Q3_C - Q1_C$), C_i is the i-th element of a specific component and N the total number of components.

Figure 7 shows the remaining data. Referring to Fig. 7a, 0.17% of the initial data have been filtered out from LOC_B PT data, whereas no outliers have been detected in LOC_A PT data. On the contrary, 16.2% and 1.6% of outliers have been identified in LOC_A T_5 and LOC_B PT data, respectively (Fig. 7b). Similar to the initial data, the LOC_A filtered values are more spread around the mean value than the LOC_B ones, presenting several outliers.

Regarding the SAT_D data, GPS_Q, SAT_U, and SAT_V have been collected for LOC_A and LOC_B (for both T_1 and T_5), computing the mean values for each location and period. From Table 3 it is possible to verify that SAT_U was the same for all the conditions, whereas the GPS_Q was *fix* for LOC_B ($GPS\_Q = 4$, fix accuracy, that is, centimeter accuracy) and *float* for LOC_A ($GPS\_Q \simeq 5$, float accuracy, that is, meter accuracy). Finally, SAT_V results show more satellites in view when the accuracy is fixed.

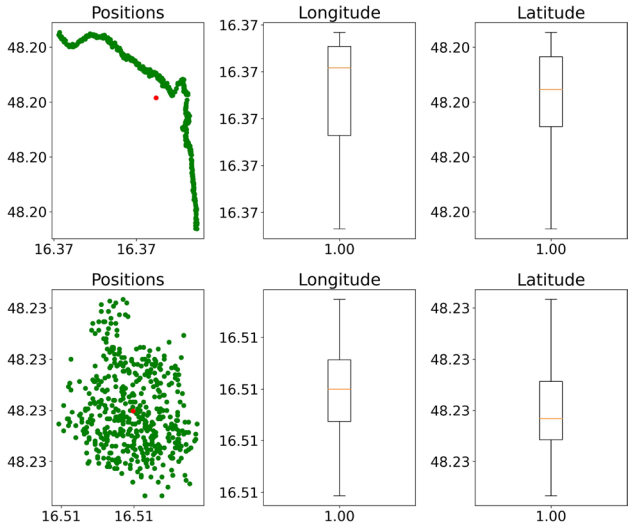

(a) PT Filtered T_1 data.

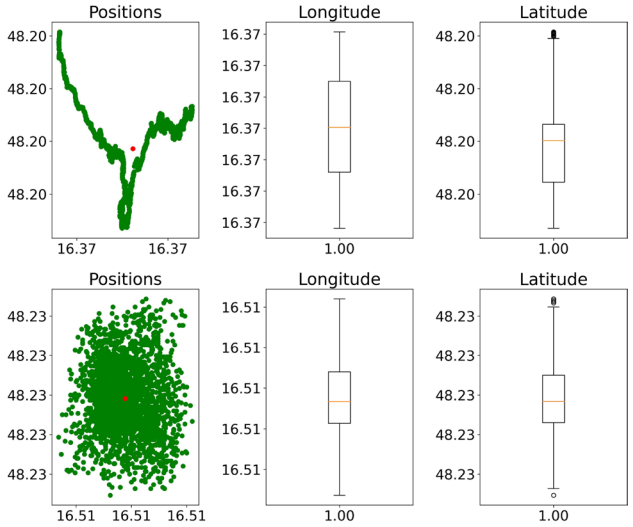

(b) PT Filtered T_5 data.

Fig. 7 The PT Filtered data. Referring to both figures, the first rows show LOC_A data, the second rows LOC_B data. The red dots (*Positions* plots) represent the mean values

Table 3 The PT SAT_D data

	SAT_U	GPS_Q	SAT_V
LOC_A T_1	12	4.97	7.18
LOC_B T_1	12	4	9.42
LOC_A T_5	12	5	7.47
LOC_B T_5	12	4	8.82

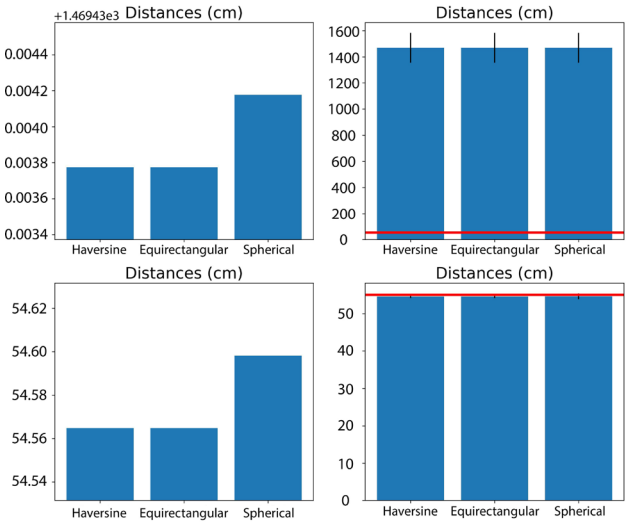

(a) Static AT DSM T_1 data.

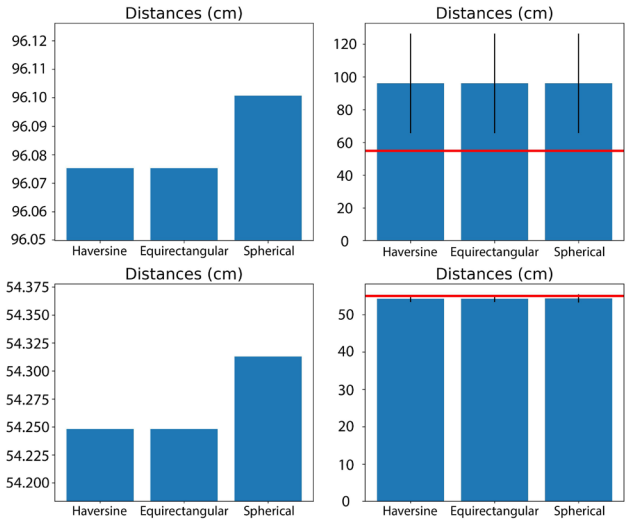

(b) Static AT DSM T_5 data.

Fig. 8 The Static AT DSM data. Referring to both figures, the first rows show LOC_A data, the second rows LOC_B data. The red horizontal lines represent the ground-truth

6.2 Static AT DSM results

Differently from PT, AT data have been collected with two RTK-GPS devices (and related smartphones, SMA_0 and SMA_1) using the DSM modality. Each device saved its positional data, used later in the post-processing analysis step to compute the relative RTK-GPS distance. Given one location, although the smartphones collected the data for the same period (T_1 or T_5) with two RTK-GPS devices running with the same update frequency (10 Hz), the number of data collected might slightly differ. This issue is due to inconsistencies in mocking the positional data, that is,

Table 4 The Static AT DSM SAT_D data

	SAT_U	GPS_Q	SAT_V
LOC_A T_1	11.43	5	8.40
LOC_B T_1	12	4	9.94
LOC_A T_5	12	4.61	8.19
LOC_B T_5	12	4	10.06

given a mock frequency update (set to 10Hz), it seems the REDCatch application cannot forward the positional data strictly complying with the specified update frequency. Hence, given the total number of samples collected by the two systems, TOT_{SMA_0} and TOT_{SMA_1}, a number of data equal to $N = min(TOT_{SMA_0}, TOT_{SMA_1})$ has been used to compute the RTG-GPS distances. As an example, during LOC_A T_1 test, SMA_0 saved 596 data whereas SMA_1 collected 595 values, thus $N = 595$. Following this logic, 595 samples were used to compute distances for LOC_A T_1, 589 for LOC_B T_1, 2979 for LOC_A T_5 and 2971 for LOC_B T_5. No missing values were detected.

Figure 8a and b show the average distances computed for T_1 and T_5, respectively. The first rows present LOC_A results, whereas LOC_B outcomes are shown in the second rows. Given one row, the first plot illustrates the average values, highlighting the three methodologies used to compute distances (Sect. 5.1.1). The second plot shows the average distance values, highlighting the gap from the ground truth ($L = 55$ cm, the red horizontal line). By qualitatively analyzing the data, it is evident that LOC_B results are much closer to the ground truth than the LOC_A ones. Moreover, for both T_1 and T_5, Eqs. 1 and 2 present similar outcomes, whereas Eq. 3 computes higher values. The LOC_A and LOC_B T_1 results have also been statistically analyzed to detect meaningful differences. The Shapiro-Wilk test reported non-normal distributions for LOC_A and LOC_B ($p_{LOC_A} < 0.001$, $p_{LOC_B} < 0.001$). Hence, the data have been analyzed using the Mann–Whitney U test, detecting statistically significant differences ($p < 0.001$) for all equations. The LOC_A T_1 outcomes are $D_H = 1469.43, D_E = 1469.43, D_S = 1469.44$ whereas LOC_B T_1 are $D_H = 54.56, D_E = 54.56, D_S = 54.59$, showing an average error of 2571% and 0.7%, respectively (average error $Error_{avg} = 100(|D - L|)/L$, with $D = (D_H + D_E + D_s)/3$ and $L = 55$). The same procedure was applied for LOC_A and LOC_B T_5 outcomes, detecting non-normal distributions ($p_{LOC_A} < 0.001$, $p_{LOC_B} < 0.001$) and statistically significant differences ($p < 0.001$) for all equations. The LOC_A T_5 distance average values are $D_H = 96.07, D_E = 96.07, D_S = 96.10$ whereas LOC_B T_5 are $D_H = 54.24, D_E = 54.24, D_S = 54.31$, showing an average error of 74 and 1.3%, respectively.

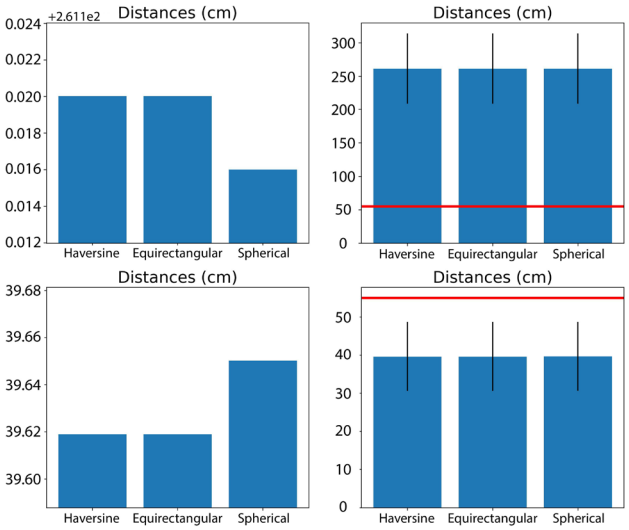

(a) Dynamic AT DSM T_1 data.

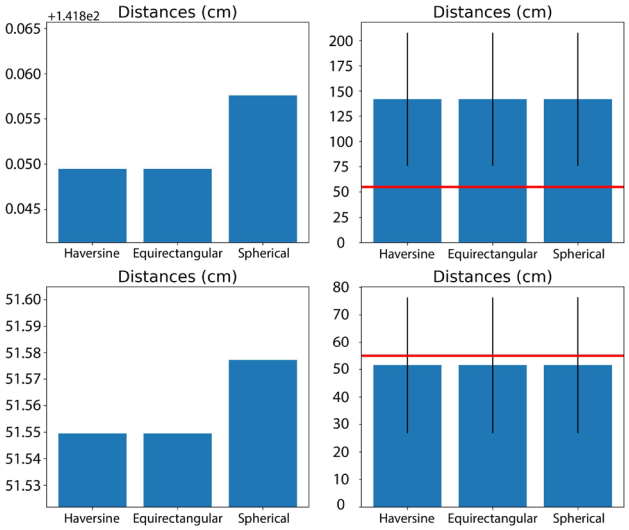

(b) Dynamic AT DSM T_5 data.

Fig. 9 The Dynamic AT DSM data. Referring to both figures, the first rows show LOC_A data, the second rows LOC_B data. The red horizontal lines represent the ground-truth

Regarding the SAT_D data, the average values of each location have been computed using the data collected with SMA_0 and SMA_1. Table 4 shows the SAT_D outcomes: during the LOC_A T_1 experiment, the GPS-RTK devices used fewer satellites than the other experiments. Similar to PT, as the number of satellites in view grows, the accuracy increases, showing that an open-sky environment provides better GPS signal quality than a high-dense urban area.

6.3 Dynamic AT DSM results

Differently from Sect. 6.2, the two RTK-GPS devices (and related smartphones) were fixed to the rotating platform (relative distance $L = 55$ cm). While the platform was rotating for 1 or 5 min (T_1 and T_5), the devices were collecting positional data using the DSM modality. Following the same logic of Sect. 6.2, 594 values were used for LOC_A T_1, 594 for LOC_B T_1, 2968 for LOC_A T_5, and 2962 for LOC_B T_5. One missing value was detected for LOC_A T_5.

Figure 9a and b illustrates the average distances for T_1 and T_5, respectively. Considering both Figures, LOC_B outcomes are closer to the L ground-truth with respect to the LOC_A ones, though they are less accurate than the static PT results (Sect. 6.2). Equations 1, 2 and 3 present outcomes consistent with PT ones but for LOC_A T_1 distances computed with Eq. 3, which tend to be higher than distances computed with Eqs. 1 and 2. LOC_A and LOC_B T_1 T_5 were not normally distributed ($p < 0.001$) and the Mann–Whitney U test detected statistically significant differences for both periods ($p < 0.001$). LOC_A T_1 distances present a greater gap from L than the LOC_B T_1 ones (LOC_A: $D_H = 261.11, D_E = 261.11, D_S = 261.13$, LOC_B: $D_H = 39.61, D_E = 39.61, D_S = 39.65$). LOC_B T_5 outcomes show a similar pattern, with LOC_B distances more accurate than LOC_A ones (LOC_A: $D_H = 141.84, D_E = 141.84, D_S = 141.86$, LOC_B: $D_H = 51.54, D_E = 51.54, D_S = 51.57$). The average LOC_A and LOC_B errors are 374%-27% (T_1) and 157%-6% (T_5), respectively.

As introduced in Sect. 5.2, dynamic DSM data have been also manually synchronized using the Unix epochs. After the synchronization, 594 values were used for LOC_A T_1, 566 for LOC_B T_1, 2942 for LOC_A T_5, and 2960 for LOC_B T_5.

Figure 10a and b shows the average distances for T_1 and T_5 computed using the synchronized data, respectively. Generally, the outcomes are consistent with the not-synchronized data, showing highly accurate distance values for LOC_B data. Specifically, the LOC_A and LOC_B T_1 T_5 samples have a non-normal distributions ($p < 0.001$) and present statistically significant differences ($p < 0.001$). The distances values for LOC_A T_1 are $D_H = 262.15, D_E = 262.15, D_S = 262.14$ whereas LOC_B T_1 are $D_H = 39.04, D_E = 39.04, D_S = 39.08$, with average errors of 376% and 29%, respectively. Considering T_5 outcomes, LOC_A distance values are $D_H = 140.39, D_E = 140.39, D_S = 140.40$ whereas LOC_B are $D_H = 51.55, D_E = 51.55, D_S = 51.58$, with average errors of 155% and 6%, respectively.

Table 5 shows the average SAT_D data, collected using the two RTK-GPS devices. The data are consistent with the previous ones, showing that the accuracy grows when the number of satellites in view increases.

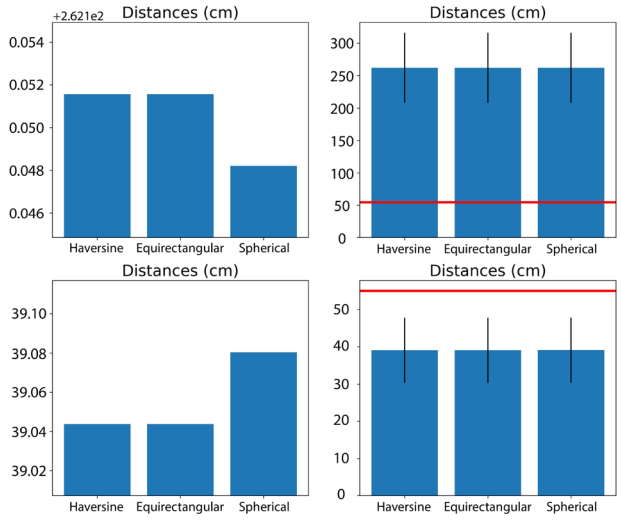

(a) Dynamic AT DSM Synchronized T_1 data.

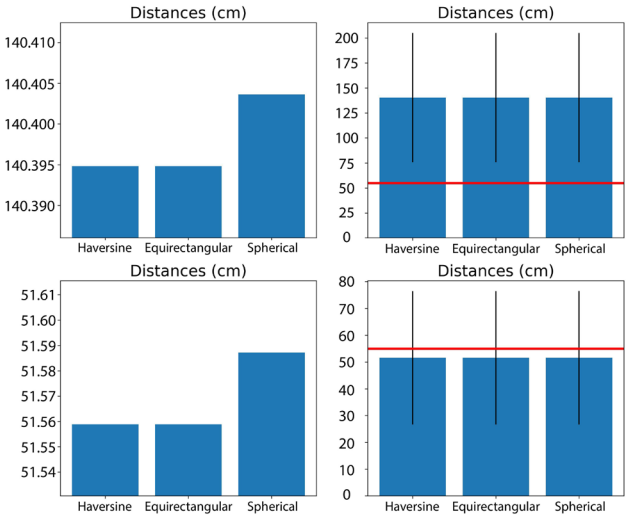

(b) Dynamic AT DSM Synchronized T_5 data.

Fig. 10 The Dynamic AT DSM Synchronized data. Referring to both figures, the first rows show LOC_A data, the second rows LOC_B data. The red horizontal lines represent the ground-truth

Table 5 The Dynamic AT DSM SAT_D data

	SAT_U	GPS_Q	SAT_V
LOC_A T_1	12	4.97	8.90
LOC_B T_1	12	4.00	10.84
LOC_A T_5	12	4.97	7.98
LOC_B T_5	12	3.93	10.85

6.4 Static AT RTM results

Data were collected using two RTK-GPS devices placed at known distance $L = 55$ cm and distances were computed in

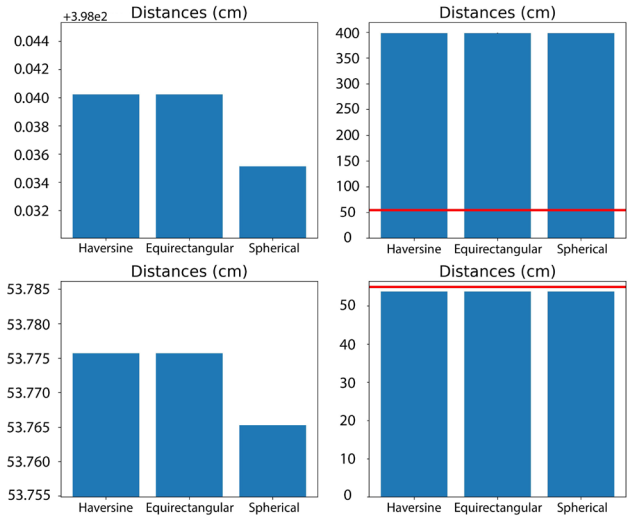

(a) Static AT RTM T_1 data.

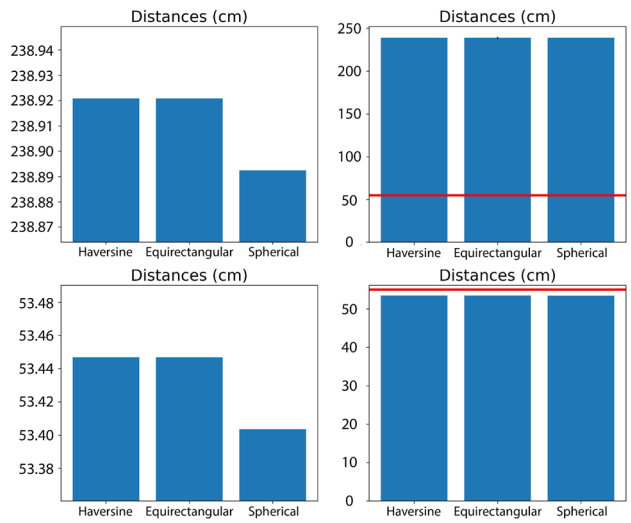

(b) Static AT RTM T_5 data.

Fig. 11 The Static AT RTM data. For both figures, first rows show LOC_A data, second rows LOC_B data. The red lines represent the ground-truth

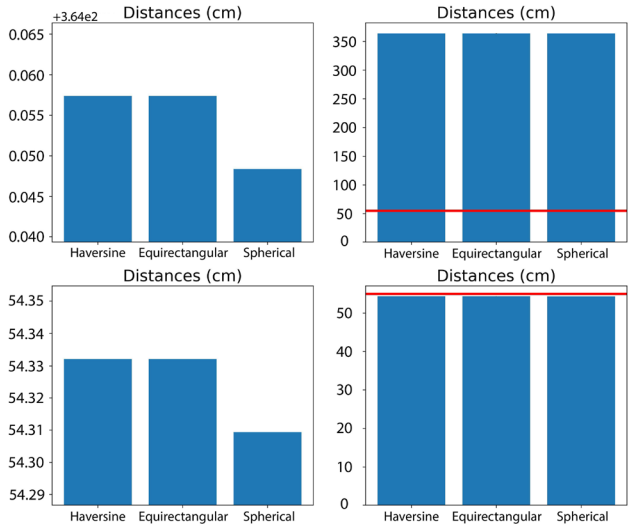

(a) Dynamic AT RTM T_1 data.

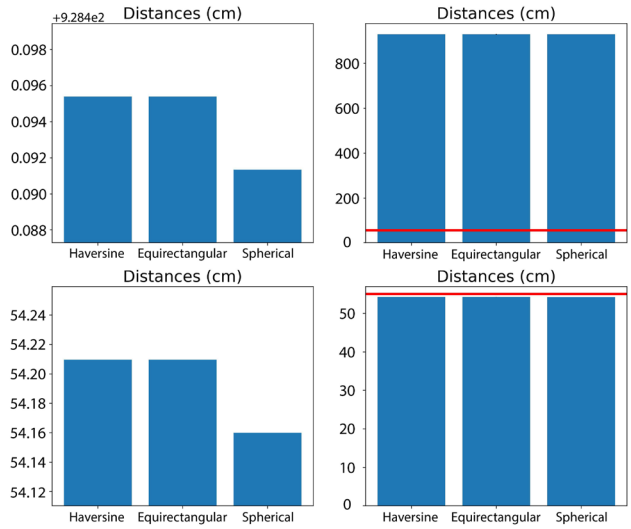

(b) Dynamic AT RTM T_5 data.

Fig. 12 The Dynamic AT RTM data. Referring to both figures, the first rows show LOC_A data, the second rows LOC_B data. The red horizontal lines represent the ground-truth

Table 6 The Static AT RTM SAT_D data

	SAT_U	GPS_Q	SAT_V
LOC_A T_1	12	5	9.36
LOC_B T_1	12	4	10.44
LOC_A T_5	12	5	9.19
LOC_B T_5	12	4	10.24

real-time by the server (see Sect. 5.1).

Figure 11a and b shows the T_1 and T_5 outcomes respectively. Similar to the results of Sect. 6.3, distances computed in LOC_A present higher values than the LOC_B ones. On the contrary, distances computed with Eq. 3 tend to be lower than distances calculated with Eqs. 1 and 2, though the difference is less than 5 mm. Data presented non-normal distributions ($p < 0.001$) and statistically significant differences ($p < 0.001$). LOC_A T_1 distances are $D_H = 398.04, D_E = 398.04, D_S = 398.03$ whereas LOC_B T_1 are $D_H = 53.77, D_E = 53.77, D_S = 53.76$, with average errors of 623 and 2%, respectively. Referring to LOC_A T_5 outcomes, distances are $D_H = 238.92, D_E = 238.92, D_S = 238.89$ whereas LOC_B T_5 are $D_H = 53.44, D_E = 53.44, D_S = 53.40$, with average errors of 76% and 3%, respectively. SAT_D data are shown

Table 7 The Dynamic AT RTM SAT_D data

	SAT_U	GPS_Q	SAT_V
LOC_A T_1	12	4.99	9.60
LOC_B T_1	12	4	10.67
LOC_A T_5	12	4.96	10.39
LOC_B T_5	12	4	8.02

in Table 6 showing a stable fix accuracy when the average number of satellites is equal to 10.

6.5 Dynamic AT RTM results

As for Sect. 6.4, data were collected with two RTK-GPS devices placed at known distance $L = 55$ cm and distances were computed in real-time by the server (Sect. 5.1). However, the platform rotated for 1 or 5 min, depending on the period (T_1 and T_5).

T_1 and T_5 outcomes are illustrated in Fig. 12a and b, respectively. Overall, the results are consistent with the previous ones, both in terms of the deviation from the ground truth and the outcomes of the distance equations. Since data were not normally distributed ($p < 0.001$), the results were analyzed with the Mann-Whitney U test which showed statistically significant differences ($p < 0.001$). LOC_A T_1 results are $D_H = 364.05, D_E = 364.05, D_S = 364.04$ whereas LOC_B T_1 are $D_H = 54.33, D_E = 54.33, D_S = 54.30$, with average errors of 561 and 1.2%, respectively. Considering the LOC_A T_5 outcomes, distances are $D_H = 928.49, D_E = 928.49, D_S = 928.48$ whereas LOC_B T_5 are $D_H = 54.20, D_E = 54.20, D_S = 54.15$, with average errors of 94 and 1.4%, respectively.

Table 7 illustrates the SAT_D data. Contrary to the previous results, an increase in the number of satellites in view does not correspond to an increase in GPS quality, showing fix accuracy when SAT_V is between 7 and 8.

7 Discussion

Referring to PT results, data collected in LOC_B are uniformly distributed around the mean value, independently of the period, even when not filtered with IQRs. On the contrary, LOC_A samples are much more inconsistent and seem to produce fake trajectories, as the RTK-GPS device was drifting over time. Independently of the location, latitude values seem more skewed than longitude ones, generating several outliers, which increase with time (especially in the LOC_A location).

The AT analysis confirms the PT outcomes, demonstrating that when the RTK-GPS device is used in open-sky areas, it can reach 1 cm accuracy. Time seems to play a vital key-role, that is, the accuracy increases independently of the location when the RTK-GPS devices are employed for long periods. For example, during the dynamic DSM not-synchronized experiments, the LOC_A and LOC_B accuracy passed from approximately 2 m to 1 m and from 16 cm to 5 mm, respectively. Generally, the SAT_D data indicate that as the number of satellites in view grows, the GPS quality increases. All the experiments show the same pattern (the accuracy improves over time and direct proportionality between the number of satellites in view and GPS quality) but for the dynamic RTM results (Sect. 6.5). In fact, LOC_A and LOC_B T_5 outcomes are less accurate than T_1 ones, and there is no relation between SAT_V and GPS_Q. At the time of writing, there is no clear explanation of this phenomenon, and future tests will be carried out to investigate the time-accuracy and SAT_V-GPS_Q relations further. Instead, it is demonstrated that the RED-Catch RTK device can achieve 1 cm accuracy when used in open-sky areas. This result has a significant impact on future developments of wearable AR outdoor tracking systems, and it is possible to define some guidelines:

- The average tracking accuracy of current wearable AR devices is approximately 2 cm (Liu et al. 2018; Soares et al. 2021). Hence, GPS-RTK devices can be used to improve the wearable AR tracking capabilities when employed in open-sky areas, far from obstacles and buildings;
- Since vSLAM techniques are not robust when used in textureless and ambiguous environments (e.g., deserts, extraterrestrial landscapes), the RTK-GPS positional data can be used to reduce the positional tracking error, thus enabling the use of wearable AR devices in environments that lack visual features;
- Contrary to mobile devices (i.e., smartphones) that can benefit from the GPS positional data when used in high-dense urban areas, the combined use of RTK-GPS and wearable AR devices is strongly discouraged in these areas as it will negatively affect the tracking accuracy of the wearable AR systems;
- When wearable AR devices are used in high-dense urban areas, it is recommended to rely only on the internal tracking capabilities of the AR systems which are accurate enough to be effectively used in such environments.

AR applications are usually used in dynamic scenarios where the users move through different conditions, passing from open-sky areas to high-dense urban environments. Hence, it becomes crucial to understand in real-time in which conditions users are in. In order to achieve this goal, it might be possible to use the GPS_Q and SAT_V messages of the NMEA protocol. A simple approach would be to use

the GPS data only *when* the GPS_Q is *fix*, thus improving the wearable AR tracking capabilities in open-sky areas.

8 Conclusion

This paper presented a rigorous evaluation of a small-size RTK device for wearable AR applications. The evaluation considered both static and dynamic conditions as well as open-sky and urban areas.

The results clearly show that the considered RTK device can achieve 1 cm accuracy in static and dynamic conditions when used in open-sky areas. On the contrary, obstacles and buildings significantly reduce the overall accuracy, passing from 1 cm to more than 10 m. These outcomes indicate that wearable AR devices can benefit from the great accuracy of the RTK devices, possibly overcoming the vSLAM drawbacks that occur in ambiguous, textureless, and repetitive environments.

In order to not negatively affect the tracking accuracy of the wearable AR device, it becomes crucial to understand *when* to use the GPS data. Hence, future works will focus on developing RTK AR wearable solutions capable of analyzing the GPS quality in real-time, avoiding negatively affecting the wearable AR tracking capabilities with inaccurate positional data.

Funding Open access funding provided by TU Wien (TUW). The research leading to these results received funding from the Austrian Research Promotion Agency (FFG) under Grant Agreement No FO999886342 KIRAS MRespond.

Data availability The dataset generated during the current study is available in the TU Data Repository, https://doi.org/10.48436/pahck-nme38.

Declarations

Conflict of interest The authors have no competing interests to declare that are relevant to the content of this article.

References

Agrawal M, Konolige K (2006) Real-time localization in outdoor environments using stereo vision and inexpensive gps. In: 18th International conference on pattern recognition (ICPR'06), vol 3, pp 1063–1068. IEEE

Bakuła M, Przestrzelski P, Kaźmierczak R (2014) Reliable technology of centimeter gps/glonass surveying in forest environments. IEEE Trans Geosci Remote Sens 53(2):1029–1038

Blanco-Pons S, Carrión-Ruiz B, Duong M, Chartrand J, Fai S, Lerma JL (2019) Augmented reality markerless multi-image outdoor tracking system for the historical buildings on parliament hill. Sustainability 11(16):4268

Chiuman N, Atunggal D, Rokhmana CA (2019)Evaluation on the performance of ntrip rtk positioning using multi-frequency low-cost gps module in areas with different telecommunication signal strength. In: 2019 5th International Conference on Science and Technology (ICST), vol 1, pp 1–4. IEEE

Fajnerová I, Greguš D, Hlinka J, Nekovářová T, Škoch A, Zítka T, Romportl J, Žáčková E, Horáček J (2018) Could prolonged usage of gps navigation implemented in augmented reality smart glasses affect hippocampal functional connectivity? BioMed research international

Feiner S, MacIntyre B, Höllerer T, Webster A (1997) A touring machine: prototyping 3d mobile augmented reality systems for exploring the urban environment. Pers Technol 1(4):208–217

Gan-Mor S, Clark RL, Upchurch BL (2007) Implement lateral position accuracy under rtk-gps tractor guidance. Comput Electron Agric 59(1–2):31–38

Gleue T, Dähne P (2001) Design and implementation of a mobile device for outdoor augmented reality in the archeoguide project. In: Proceedings of the 2001 conference on Virtual reality, archeology, and cultural heritage, pp 161–168

Guarese RLM, Maciel A (2019) Development and usability analysis of a mixed reality gps navigation application for the microsoft hololens. In: Computer Graphics International Conference, pp 431–437. Springer

Han J-G, Park K-W, Ban K-J, Kim E-K (2013) Cultural heritage sites visualization system based on outdoor augmented reality. Aasri Procedia 4:64–71

Hegarty CJ (2017) The global positioning system (gps). In: Springer Handbook of Global Navigation Satellite Systems, pp 197–218. Springer

Henkel P, Mittmann U, Iafrancesco M (2016) Real-time kinematic positioning with gps and glonass. In: 2016 24th European Signal Processing Conference (EUSIPCO), pp 1063–1067. IEEE

Höllerer T, Feiner S, Terauchi T, Rashid G, Hallaway D (1999) Exploring mars: developing indoor and outdoor user interfaces to a mobile augmented reality system. Comput Graph 23(6):779–785

Isrie S, Moonen N, Schipper H, Bergsma H, Leferink F (2018) Measuring, logging, and visualizing pulsed electromagnetic fields combined with gps location information. In: 2018 international symposium on electromagnetic compatibility (EMC EUROPE), pp 500–505. IEEE

Jakus G, Guna J, Tomažič S, Sodnik J (2014) Evaluation of leap motion controller with a high precision optical tracking system. In: Human-Computer Interaction. Advanced Interaction Modalities and Techniques: 16th International Conference, HCI International 2014, Heraklion, Crete, Greece, Jun 22–27, 2014, Proceedings, Part II 16, pp 254–263. Springer

Kamat VR, Behzadan AH (2006) Gps and 3dof tracking for georeferenced registration of construction graphics in outdoor augmented reality. In: Workshop of the European Group for Intelligent Computing in Engineering, pp 368–375. Springer

Kluga A, Mitrofanovs I, Kluga J, Jeralovics V (2014) State and dynamic precision research using two gps receivers with rtk. In: 2014 14th Biennial Baltic Electronic Conference (BEC), pp 141–144. IEEE

Kurkovsky S, Koshy R, Novak V, Szul P (2012) Current issues in handheld augmented reality. In: 2012 international conference on communications and information technology (ICCIT), pp 68–72. IEEE

Ling FF, Elvezio C, Bullock J, Henderson S, Feiner S (2019) A hybrid rtk gnss and slam outdoor augmented reality system. In: 2019 IEEE Conference on Virtual Reality and 3D User Interfaces (VR), pp 1044–1045. IEEE

Liu Y, Dong H, Zhang L, El Saddik A (2018) Technical evaluation of hololens for multimedia: a first look. IEEE MultiMedia 25(4):8–18

Lucero-Urresta E, Buele J, Córdova P, Varela-Aldás J (2021) Precision shooting training system using augmented reality. In: International Conference on Computational Science and Its Applications, pp 283–298. Springer

Muhammed RR, AS Mahdi (2018) Accurate three dimensional coordinates measurements using differential gps real time kinematic mode. Iraqi J Sci 59(2C):1146–1151

Mekni M, Lemieux A (2014) Augmented reality: applications, challenges and future trends. Appl Comput Sci 20:205–214

Menozzi A, Clipp B, Wenger E, Heinly J, Dunn E, Towles H, Frahm J-M, Welch G (2014) Development of vision-aided navigation for a wearable outdoor augmented reality system. Proc IEEE/ION PLANS 2014:760–772

Morales Y, Tsubouchi T (2007) Dgps, rtk-gps and starfire dgps performance under tree shading environments. In: 2007 IEEE International Conference on Integration Technology, pp 519–524. IEEE

Nazri NIAM, Rambli DRA (2014) Current limitations and opportunities in mobile augmented reality applications. In: 2014 International Conference on Computer and Information Sciences (ICCOINS), pp 1–4. IEEE

Ng K, Johari J, Abdullah S, Ahmad A, Laja B (2018) Performance evaluation of the rtk-gnss navigating under different landscape. In: 2018 18th International Conference on Control, Automation and Systems (ICCAS), pp 1424–1428. IEEE

Niu Z, Zhao X, Sun J, Tao L, Zhu B (2020) A continuous positioning algorithm based on rtk and vi-slam with smartphones. IEEE Access 8:185638–185650

Odolinski R, Teunissen PJ (2017) Low-cost, high-precision, single-frequency gps-bds rtk positioning. GPS Solut 21(3):1315–1330

Odolinski R, Teunissen PJ, Odijk D (2015) Combined bds, galileo, qzss and gps single-frequency rtk. GPS Solut 19(1):151–163

Piekarski W, Avery B, Thomas BH, Malbezin P (2003) Hybrid indoor and outdoor tracking for mobile 3d mixed reality. In: The Second IEEE and ACM International Symposium on Mixed and Augmented Reality, 2003. Proceedings., pp 266–266. Citeseer

Pintaric T, Kaufmann H (2007) Affordable infrared-optical pose-tracking for virtual and augmented reality. In: Proceedings of Trends and Issues in Tracking for Virtual Environments Workshop, IEEE VR, pp 44–51

Pombo L, Marques MM, Afonso L, Dias P, Madeira J (2019) Evaluation of a mobile augmented reality game application as an outdoor learning tool. Int J Mob Blend Learn (IJMBL) 11(4):59–79

Reitmayr G, Drummond TW (2006) Going out: robust model-based tracking for outdoor augmented reality. In: 2006 IEEE/ACM international symposium on mixed and augmented reality, pp 109–118. IEEE

Safrel I, Julianto EN, Usman NQ (2018) Accuracy comparison between gps real time kinematic (rtk) method and total station to determine the coordinate of an area. Jurnal Teknik Sipil Dan Perencanaan 20(2):123–130

Schall G, Wagner D, Reitmayr G, Taichmann E, Wieser M, Schmalstieg D, Hofmann-Wellenhof B (2009) Global pose estimation using multi-sensor fusion for outdoor augmented reality. In: 2009 8th ieee international symposium on mixed and augmented reality, pp 153–162. IEEE

Singh S, Ma Z, Giunchi D, Steed A (2020) Real-time collaboration between mixed reality users in geo-referenced virtual environment. arXiv preprint arXiv:2010.01023

Soares I, Sousa RB, Petry M, Moreira AP (2021) Accuracy and repeatability tests on hololens 2 and htc vive. Multimod Technol Interact 5(8):47

Speroni EA, Ceolin SR, dos Santos OM, Legg AP (2018) A low cost vslam prototype using webcams and a smartphone for outdoor application. In: Proceedings of the 33rd Annual ACM Symposium on Applied Computing, pp 268–275

Stranner M, Arth C, Schmalstieg D, Fleck P (2019) A high-precision localization device for outdoor augmented reality. In: 2019 IEEE International Symposium on Mixed and Augmented Reality Adjunct (ISMAR-Adjunct), pp 37–41. IEEE

Sutherland IE (1968) A head-mounted three dimensional display. In: Proceedings of the December 9-11, 1968, fall joint computer conference, part I, pp 757–764

Tache R, Abeykoon HA, Karunanayaka KT, Kumarasinghe JP, Roth G, Fernando ONN, Cheok AD (2012) Command center: authoring tool to supervise augmented reality session. In: 2012 IEEE Virtual Reality Workshops (VRW), pp 99–100. IEEE

Taketomi T, Uchiyama H, Ikeda S (2017) Visual slam algorithms: a survey from 2010 to 2016. IPSJ Trans Comput Vis Appl 9(1):1–11

Teunissen P, Odolinski R, Odijk D (2014) Instantaneous beidou+ gps rtk positioning with high cut-off elevation angles. J Geodesy 88(4):335–350

Thomas B, Close B, Donoghue J, Squires J, De Bondi, M. Morris P, Piekarski W (2000) Arquake: An outdoor/indoor augmented reality first person application. In: Digest of Papers. Fourth International Symposium on Wearable Computers, pp 139–146. IEEE

Tomaszewski D, Wielgosz P, Rapiński J, Krypiak-Gregorczyk A, Kaźmierczak R, Hernández-Pajares M, Yang H, OrúsPérez R (2020) Assessment of centre national d'ètudes spatiales real-time ionosphere maps in instantaneous precise real-time kinematic positioning over medium and long baselines. Sensors 20(8):2293

Ungureanu D, Bogo F, Galliani S, Sama P, Duan X, Meekhof C, Stühmer J, Cashman TJ, Tekin B, Schönberger JL, et al (2020) Hololens 2 research mode as a tool for computer vision research. arXiv preprint arXiv:2008.11239

Van Krevelen D, Poelman R (2010) A survey of augmented reality technologies, applications and limitations. Int J Virt Real 9(2):1–20

Wiśniewski B, Bruniecki K, Moszyński M (2013) Evaluation of rtklib's positioning accuracy usingn low-cost gnss receiver and asg-eupos. TransNav: Int J Mar Navigat Saf Sea Transp 7(1):79–85

Zari G, Condino S, Cutolo F, Ferrari V (2023) Magic leap 1 versus microsoft hololens 2 for the visualization of 3d content obtained from radiological images. Sensors 23(6):3040

Zhang Y, Yu W, Han Y, Hong Z, Shen S, Yang S, Wang J (2019) Static and kinematic positioning performance of a low-cost real-time kinematic navigation system module. Adv Space Res 63(9):3029–3042

Zheng Y, Birdal T, Xia F, Yang Y, Duan Y, Guibas LJ (2022) 6d camera relocalization in visually ambiguous extreme environments. arXiv preprint arXiv:2207.06333